Renewable Energy, Environment, and Power Quality Journal (REE&PQJ)
ISSN:3020-531X
Volume 26, July 2026

Inverter-Based Power Flow Control of a Small-Scale Grid-Connected Doubly-Fed Induction Generator in Wind Energy Conversion Systems Under Variable Wind Speed Conditions

Milkias Berhanu Tuka[1,2], Anatoli Wellhöfer[3]

[1]Alexander von Humboldt Foundation Postdoctoral Research Fellowships Programme,
Technical University of Applied Sciences Würzburg-Schweinfurt (THWS), Schweinfurt, Germany
[2]Addis Ababa Science and Technology University, Addis Ababa, Ethiopia

[3]Technical University of Applied Sciences Würzburg-Schweinfurt (THWS), Schweinfurt, Germany
Ignaz-Schön-Straße 11, 97421 Schweinfurt, Germany
milkias.berhanu@aastu.edu.et, anatoli.wellhoefer@thws.de

Abstract. Inverters are critical components in wind turbine-based energy conversion systems, serving essential roles in control and grid synchronization under dynamic conditions. This paper presents an inverter-based power flow control using PI controller with an anti-windup mechanism for a small-sized 1 kW Doubly-Fed Induction Generator (DFIG), addressing a gap in the literature where the dynamic behavior of such systems is often insufficiently described. The control strategy is integrated with a Maximum Power Point Tracking (MPPT) algorithm. Key real-time machine parameters were derived from experimental tests. To evaluate controller robustness, the system was subjected to a random variation of wind speeds within a comprehensive grid-connected DFIG-based Wind Energy Conversion System (WECS) model. A key contribution and novelty of this work is its reliance on real machine parameters and modes for an in-depth performance analysis conducted using the latest MATLAB/Simulink 2025b environment. The findings indicate that the machine reaches its rated power at approximately 8.5 m/s wind speed at 0° pitch angle under MPPT control in effectively regulating and tracking active and reactive power flows independently, while the cut-in speed is 4 m/s. These findings indicate the machine's suitability for its operation in small-scale grid-connected or micro-grid systems tailored to specific site conditions.

Key words. Doubly-Fed Induction Generator, MATLAB/Simulink, Power Flow Control, PI Controller, Variable Wind Speed

1. Introduction

The wind power-based renewable energy integration in the power sector is playing a greater role nowadays due to its continuous developments in size and control aspects. A global increment in the integration of wind energy into the national grids, as per the GWEC's 2026 report, indicates that around 150 GW of new power is installed in the year 2025 with a significant increment to cope with the 2030 agenda with the new record [1]. The same report notes that, although this new record marks a major step forward, it still represents only about half of the annual capacity needed by 2030 to remain aligned with net-zero pathways. The swift expansion of wind energy-based renewable energy, especially the integration of wind farms into existing power networks, has become a central pillar in the global transition toward sustainable energy systems [2]. This transition also accelerates technological progress, encouraging innovations that enhance the competitiveness and affordability of wind energy within an evolving energy market. Global demand for renewable energy, with wind power installation is expected to steadily rise in the world up-to 19 % by 2030 and 20-25 % by 2050 [3]. Besides these developments in the wind power industry, a grid-tied DFIG via its stator, as shown in Fig.1, is the most widely used generator nowadays, dominating major sectors [1].

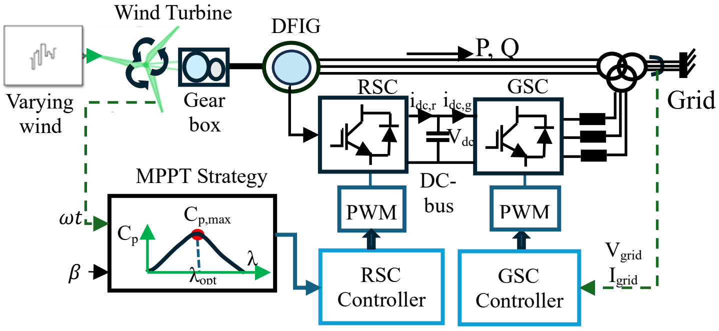

Fig. 1. Grid-connected DFIG with dual-back-to-back converters.

However, despite these advancements, there exists a significant challenges across grid-connected wind power systems including an accurate modeling and control of wind turbine generators under steady-state, dynamic, and short-circuit conditions; maintaining grid stability, reliability, and power quality; ensuring effective protection coordination;

complying with increasingly stringent grid-code requirements; and developing robust control algorithms capable of reliably tracking maximum power point tracking (MPPT) operation [4-6].

Thus, this paper addresses the DFIG-based Wind Energy Conversion System (WECS) with an accurate modelling in a user-defined function block set of a the latest MATLAB/Simulink 2025b software under dynamic wind conditions by designing a PWM inverter under the stator flux frame of orientation for the Rotor Side Converter (RSC) and voltage orientation for the Grid Side Converter (LSC) using the actual machine parameters determined from the test reports and name plate data of 1kW machine in the Lab of THWS as shown in Appendix. The Maximum Power Point Tracking (MPPT) algorithms have been developed to capture the most out of the existing wind. The gains of the controller are determined from the real machine parameters. Overall, this work contributes by optimizing the performance of a small-scale wind machine using MPPT algorithms and demonstrating its suitability for grid-integration applications, an area that remains insufficiently addressed in existing literature [7]-[9]. A complete set of machine parameters has been identified, enabling the derivation of accurate control gains based on real experimental data. Furthermore, the study can be extended to evaluate the machine's behavior under various fault conditions, different wind-speed scenarios, and evolving grid-code requirements. The findings, therefore, offer valuable insights and practical approaches for addressing key challenges associated with the grid integration of small-scale wind energy systems.

2. Design and Modelling

This section describes design and modelling approaches of the grid-tied WECS systems.

A. *Inverter Design and Modelling*

Inverters are among the most important elements in WECS, playing greater roles in synchronizing and controlling power flows. Fig. 2 shows a single-phase inverter with the load and its switching pattern.

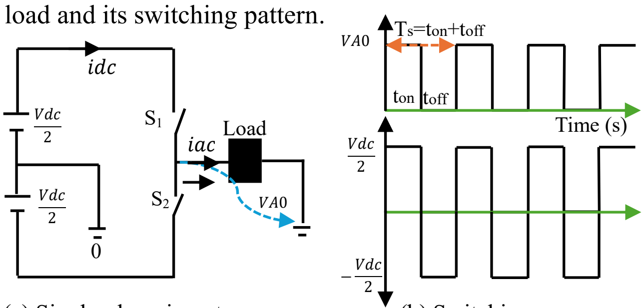

(a) Single-phase inverter (b) Switching

Fig. 2. Single-phase inverter and its switching

Where vdc is the DC voltage, Ts is the switching time of the inverter, and V_{A0} is the phase voltage.

The $vA0$can be described as (1), and its magnitude can be determined as given in (2).

$$v_{A0} = \begin{cases} \frac{V_{dc}}{2}, & S_1 = 1,\ S_2 = 0 \\ -\frac{V_{dc}}{2}, & S_1 = 0,\ S_2 = 1 \end{cases} \quad (1)$$

$$\bar{v}A0 = \frac{1}{T_s}\int_0^{T_s} v_{A0}dt = \frac{1}{T_s}[\int_0^{T_{on}} v_{A0}dt$$

$$= \int_{T_{on}}^{T_s} v_{A0}dt + \frac{v_{dc}}{2T_s}[T_{on} - T_s + T_{on} = \frac{v_{dc}}{2}(2d-1) \quad (2)$$

Where, d= $\frac{T_{on}}{T_s}$ is the duty cycle, which is equivalent to the on/off behavior of the power switches. Thus, (2) in terms of three-phase systems can be further rewritten as:

$$\bar{v}A0 = \frac{V_{dc}}{2}(2S_{123} - 1) \quad (3)$$

$$i_{dc123} = S_{123}i_{ac} \quad (4)$$

Thus, from the phase voltage, d is determined as (5)

$$d = \frac{\bar{v}A0}{V_{dc}} + \frac{1}{2} \quad (5)$$

Inverters use the duty cycles, which refer to the proportion of time a switch is ON during one switching period, to control the output waveforms. The inverter's duty cycle, which varies from zero to one, together with its MATLAB/Simulink model shown in Fig. 3(a) and (b), is used in the study to synthesize AC sinusoidal waveforms from a DC source using Pulse Width Modulation (PWM). The detail of the approach is described in this section.

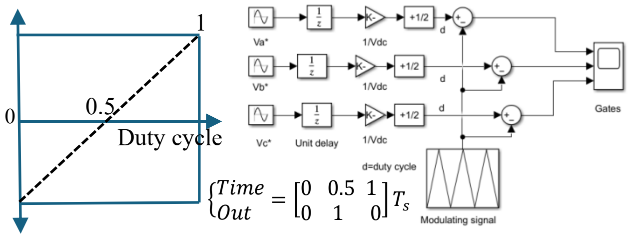

a) Duty cycles (b) Duty cycle model

Fig. 3. Duty cycle model

Thus, the complete three-phase PWM inverter model, including delay compensation to accurately represent the real system, as shown in Fig. 4, implemented in MATLAB/Simulink, is used in this study, assuming positive AC and DC currents flow out of the converter.

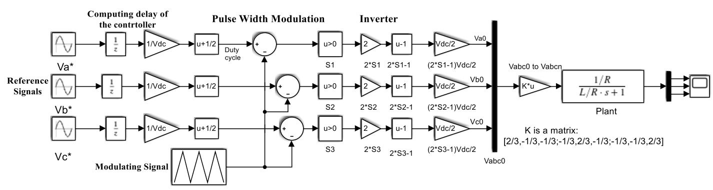

Fig. 4. Three-phase inverter system with delay compensation

Where $S_1 = 1$ if $V_a^* \geq V_{tri}$; $S_1 = 0$ if $V_a^* < V_{tri}$; $S_2 = 1$ if $V_b^* \geq V_{tri}$; $S_2 = 0$ if $V_b^* < V_{tri}$; $S_3 = 1$ if $V_c^* \geq V_{tri}$; $S_3 = 0$ if $V_c^* < V_{tri}$

The unit delay $(\frac{1}{z})$ in the model simulation is being used to compute the delay of the controller.

B. *Control Loops and DFIG Modelling*

The DFIG is coupled with the wind turbine rotor via its shaft and gearbox in real-time applications. The dynamic behaviors of the machine under varying wind speed conditions to track its power transfer capabilities can be best described with a properly developed model. For this study, to carry out the control of complex dynamic sequences, space vector representations of a synchronously rotating frame give the voltage expressions as described in (6) and (7) [10], [11]:

$$\vec{V}_s^a = \vec{I}_s^a R_s + \frac{d\vec{\psi}_s^a}{dt} + j\vec{\omega}_s^a \rightarrow \begin{cases} v_{ds} = R_s i_{ds} + \frac{d\psi_{ds}}{dt} - \omega_s \psi_{qs} \\ v_{qs} = R_s i_{qs} + \frac{d\psi_{qs}}{dt} + \omega_s \psi_{ds} \end{cases} \quad (6)$$

$$\vec{V}_r^a = \vec{I}_r^a R_r + \frac{d\vec{\psi}_r^a}{dt} + j\vec{\omega}_r^a \rightarrow \begin{cases} v_{dr} = R_r i_{dr} + \frac{d\psi_{dr}}{dt} - \omega_r \psi_{qr} \\ v_{qr} = R_r i_{qr} + \frac{d\psi_{qr}}{dt} + \omega_r \psi_{dr} \end{cases} \quad (7)$$

Where $\omega_m = \omega_s - \omega_r$

The corresponding space vectors are represented by a, r, and s as subscripts to indicate the synchronous, rotor, and stator reference frames, respectively.

Accordingly, the stator and rotor flux linkages represented as space vectors in the stationary reference frame can be written as in (8), as reported in [12], [13].

$$\begin{bmatrix} \Psi_s{}^a \\ \Psi_r{}^a \end{bmatrix} = \begin{bmatrix} L_s & L_m \\ L_m & L_r \end{bmatrix} \cdot \begin{bmatrix} i_s{}^a \\ i_r{}^a \end{bmatrix} \rightarrow \begin{cases} \Psi_{ds} = L_s i_{ds} + L_m i_{dr} \\ \Psi_{qs} = L_s i_{qs} + L_m i_{qr} \\ \Psi_{dr} = L_m i_{ds} + L_r i_{dr} \\ \Psi_{qr} = L_m i_{qs} + L_r i_{qr} \end{cases} \quad (8)$$

Upon inverse transform on (8), the stator currents taking self (L_{sr}) and mutual (L_m) inductances into account are given by (9):

$$\begin{bmatrix} i_s{}^a \\ i_r{}^a \end{bmatrix} = \frac{1}{L_m{}^2 - L_s . L_r} \begin{bmatrix} -L_r & L_m \\ L_m & -L_s \end{bmatrix} \begin{bmatrix} \Psi_s{}^a \\ \Psi_r{}^a \end{bmatrix} \quad (9)$$

Alongside, the real (P_s) and reactive (Q_s) powers of the stator are determined using (10) and (11), while (12) indicates the DFIG's electromagnetic torque [5].

$$P_s = \frac{3}{2}[v_{ds} i_{ds} + v_{qs} i_{qs}] \quad (10)$$

$$Q_s = \frac{3}{2}[v_{qs} i_{ds} - v_{ds} i_{qs}] \quad (11)$$

$$T_{em} = \frac{3}{2}[\psi_{dr} i_{qs} - \psi_{qr} i_{ds}] \quad (12)$$

By considering the mechanical load torque (Tm) applied to the machine shaft arising from wind-speed variations, the dynamic motion of the system is described by (13):

$$T_m - T_{em} = J\frac{d\omega_m}{dt} \quad (13)$$

The vector control is among the commonly used methods and offers an efficient control strategy that has proven its effectiveness in handling the non-linearities of wind nature [14]-[16] and is hence used in this study, as this approach is used to adapt and mitigate the problematic control situation of the WECS with DFIG. Under a considered rotating reference frame, the position of random rotating flux (e.g, φ_k) drawn as displayed in Fig. 5 is used in the modeling.

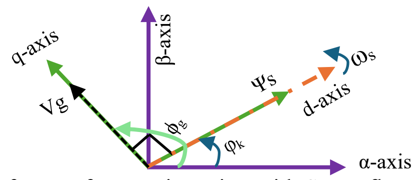

Fig. 5. Reference frame orientation with Stator flux

Taking φ_k as an assumed position of rotating flux, its magnitude can be given as (14):

$\varphi_k = \phi_g - \pi/2$, where $\phi_g = \text{atan2}(V_\beta/V_\alpha)$ (14)

The grid voltage is proportional to the stator flux during the steady state of operation [17], [18], and hence the resistance of stator winding can be neglected, yielding V_{ds}=0.

However, for dynamic conditions of the machine, including faults, voltage disturbances, and transient stability studies, stator resistance and stator flux dynamics must be considered for accurate results [19].

Under the aim of machine control during dynamic conditions, previous equations in the dq-axis of stator currents can be rewritten as (15) and (16):

$$i_{ds} = \frac{Vg}{L_s\omega_s} - \frac{L_m}{L_s} i_{dr} \quad (15)$$

$$i_{qs} = -\frac{L_m}{L_s} i_{qr} \quad (16)$$

Accordingly, the rotor dq-axis currents in terms of PQ_s powers result in (17) and (18):

$$i_{qr} = -\frac{2}{3}\frac{L_s}{V_g L_m} P_s \quad (17)$$

$$i_{dr} = \frac{V_g}{L_m\omega_s} - \frac{2}{3}\frac{L_s}{V_g L_m} Q_s \quad (18)$$

These equations show how the independent control of the stator active and reactive power of the DFIG in WECS is possible via i_{qr} and i_{dr}, respectively, with respect to individual set values, where various grid owners demand.

A unity power factor of operation can reduce the burden on the grid, simplify voltage management, and minimize the converter loading [20], [21], and hence this is used in the MATLAB/Simulink model of this study as discussed in the results sections. However, depending on specific site applications, it may also be necessary to operate the machine at non-zero reactive power levels, such as during unbalanced voltage conditions or as required by grid-code demands. Furthermore, in small and medium-scale DFIGs, operating the machine at unity power factor improves the system's electrical efficiency since the converter operates with lower current and reduced reactive power processing. This also helps to meet steady-state requirements for some grid operators.

The control scheme used in this study implements the RSC to provide unity power factors and active power at the optimum power point by tracking the wind speed and wind turbine rotor speed (ω_t), as shown in Fig. 6, while the LSC controls the DC link voltage and hence ensures control of active and reactive power flows between grids [22].

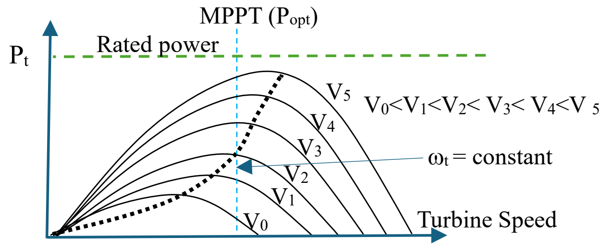

Fig. 6. Wind turbine characteristic for maximum power extraction

Under MPPT controller algorithms, the extracted wind energy power is limited by the nonlinear power coefficient, C_p, as a function of both the tip speed ratio, λ, and the pitch angle, β, which represents the efficiency of converting energies. Typically, C_p reaches its maximum at a specific λ_{opt} optimal, so the goal of the MPPT controller is to dynamically keep the rotor at a specific speed so that the turbine operates at or near this optimal λ [23]. Thus, λ_{opt} can be expressed by (23), where R is the blade's radius.

$$\lambda opt = R\omega_t / v_w \quad (19)$$

By neglecting the stator and rotor windings losses and saturations, while considering a positive AC is outgoing from the converter and a DC enters the DC-bus, the model built in a user-defined function block of the MATLAB/Simulink as a masked diagram for RSC with MPPT and current control loops shown in Fig. 7 is used.

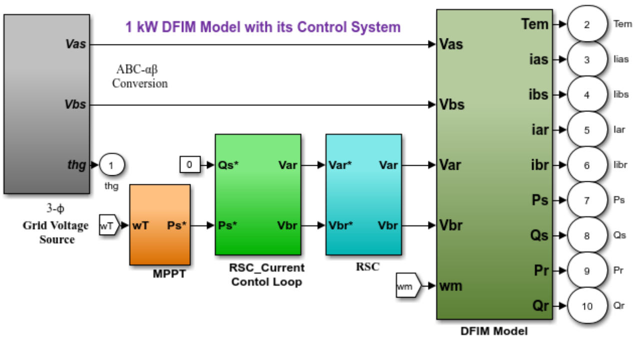

Fig. 7. DFIG and RSC controller under MPPT algorithm

Maintaining proper control of the DC-Bus voltage in a grid-connected DFIG-based WECS will be important for the converter's necessary operations, having sufficient DC-bus voltage for its proper control and synchronization operations, along with other instructed demands. In this regard, the grid voltage orientation, used for Line Side Converter (LSC) control, measures the stator voltages and aligns the q-axis with the voltage space vector, with the d-axis shifted 90^0 from it [24]. In this study, a balanced three-phase grid voltage is assumed in the simulation work, and the transformer's grid-side impedance is neglected. In the VOC implementation scheme for the LSC, the d-axis of the synchronous reference frame is aligned with the grid-voltage vector. Having a complete DFIG model with a two-level converter, control loops model, along with the other components in a WECS, as shown in Fig. 7, the next section discusses the results of the study.

3. Results and Discussions

In this study, all mathematical models of the machine, together with the associated control strategies and parameter-tuning, were implemented in the MATLAB/Simulink 2025b environment to evaluate system performance under different wind conditions. A representative, variable wind profile-comprising the sequence [4, 6, 8, 10, 8, 6, 4] m/s was applied to the wind turbine, with each wind speed maintained for a 4-seconds interval using a repeating-sequence block over a total simulation period of 52 seconds as shown in Fig. 8.

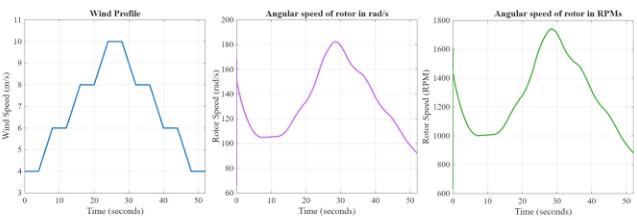

(a) Wind speeds (b) Response in rad/s (c) Response in RPM

Fig. 8. Wind profile and generator speeds

As expected, the machine speed transitions between sub-synchronous and super-synchronous operating modes in response to the varying wind input, which in turn produces corresponding variations in the total generated power. Electrical power output is mainly dependent upon generator speed. Thus, even when maximum mechanical wind power is available, the maximum electrical output cannot be guaranteed unless the corresponding optimal rotor speed is achieved [25], [26]. For this purpose, rotor speed at a given wind profile plays a crucial role in achieving the maximum power, and tracking its pattern will show us the power control regions.

Because voltage variations are directly influenced by changes in real and reactive power, particularly in weak grids where the voltage is not rigidly maintained, the DFIG may be required to inject or absorb reactive power in accordance with grid-code specifications to support voltage regulation and system stability [27]. Consequently, the adoption of established control methods used with back-to-back converters in DFIG-based systems will play a more significant role. For the applied wind speed condition, Fig. 9 presents the RMS value of the grid voltage, together with the stator flux and currents.

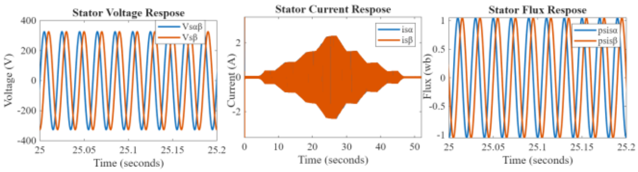

(a) Stator voltages in αβ (b) stator currents in αβ (c) Stator flux in αβ

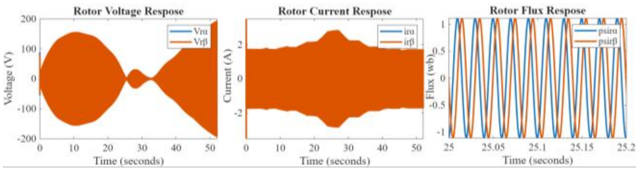

(d) Rotor voltages in αβ (e) Rotor currents in αβ (c) Rotor flux in αβ

Fig. 9. Stator and Rotor voltages, currents, and flux responses

From the above results, it can be seen that the three-phase sinusoidal and stationary, αβ stator voltages, frequency, phase angles, and fluxes are regulated to achieve synchronization with the grid, and generator amplitude is also regulated automatically, being not modified during wind speed changes, as its dependence on speed is null. However, to carry out the changing electrical power transfer resulting from the changing power in the wind, it is seen that the stator current varies. In contrast to the stator voltage, the changes in the wind speed result in the rotor voltage being 180^0 phase shifted at 24 s of the simulation period, where the higher wind speed change occurs, bringing the generator speed change to super synchronous mode of operation.

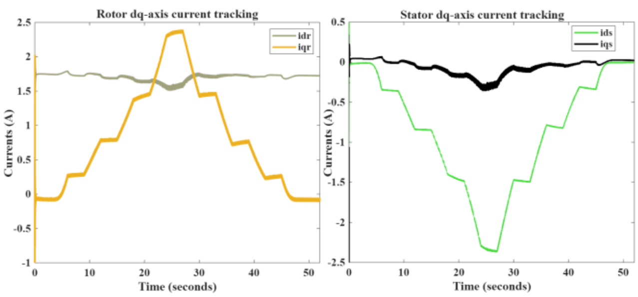

(a) Rotor dq currents (b) stator dq currents

Fig. 10. Rotor and stator dq-currents

The αβ stator and rotor fluxes remain unchanged during the simulation period, indicating that the grid voltage is nearly constant. Therefore, the control loops are fast and well-tuned, and hence the rotor flux is forced to follow its reference, which is typically constant. The rated current of the DFIG is 2 A as given in the appendix, and the simulation results validate it as shown in Fig. 10 (b) for the stator and rotor dq-axis currents at a wind speed of nearly 8.5m/s.

The rotor dq-currents shown in Fig. 10 (a) reflect an independent control of real and reactive powers as demanded by grid code operators. In this regard, RSC is used to control stator active power (P_s) by using rotor currents in q-axis as shown in Fig. 11 (a) and reactive power (Q_s) via rotor currents in d-axis (Fig. 11 (b).

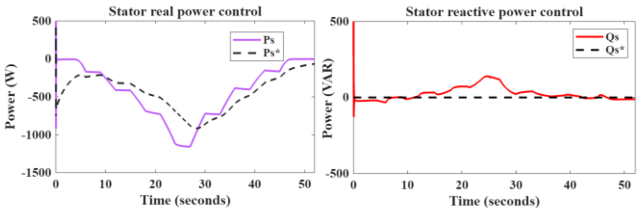

(a) Stator's real power control (b) Stator reactive power control
Fig. 11. Tracking of stator's real and reactive powers under MPPT

The current controller loop references remain bounded and smooth without significant chattering for the control of active and reactive power flows between the grid and machine. Similarly, Fig. 12 shows the DC currents between the DC-bus and the rotor voltages in the dq-axis and the corresponding real-reactive power of the rotor of the DFIG.

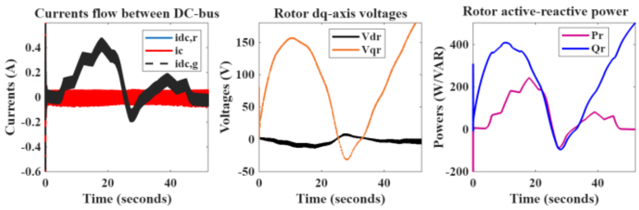

(a) DC-Bus currents (b) Rotor Voltages (c) Rotor active-reactive power
Fig. 12. DC-bus currents, rotor voltages, and powers

Consequently, the difference between the two currents through the capacitor remains nearly the same as expected under DC-Bus voltage regulation for the rotor dq-axis voltages shown in Fig. 12 (a).

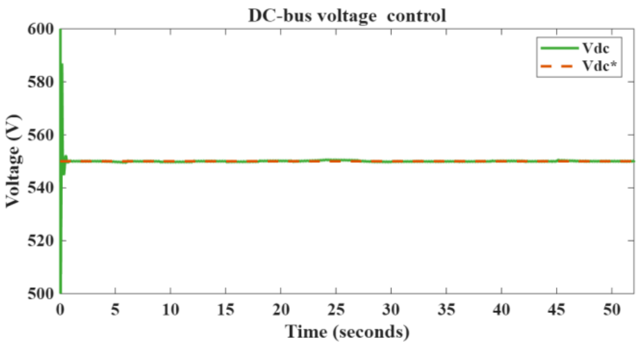

Fig. 13. DC link voltage control

As the rotor voltage is dependent on the relative motion between the rotor and the stator flux, operation in the super-synchronous region basically reduces this relative motion because the rotor speed increases and the slip magnitude decreases. This negative rotor voltage reflects the reversal of power flow through the rotor circuit, meaning that power is injected from the RSC back into the grid. As a result, the total electrical power delivered to the grid will increase. Fig. 13 shows the DC-bus voltage regulation under a given set of wind conditions. The DC-bus voltage for the machine is set at 550 V, and the controller is designed accordingly.

The perfect tracking of the DC-bus voltage, as shown in Fig. 13, is a good indication of how closely the measured DC-Bus voltage follows its reference under varying wind speeds. The current controller loops output of the LSC references remains bounded and smooth without significant chattering, as shown in Fig. 14 for the control of active and reactive power flows between the grid and machine.

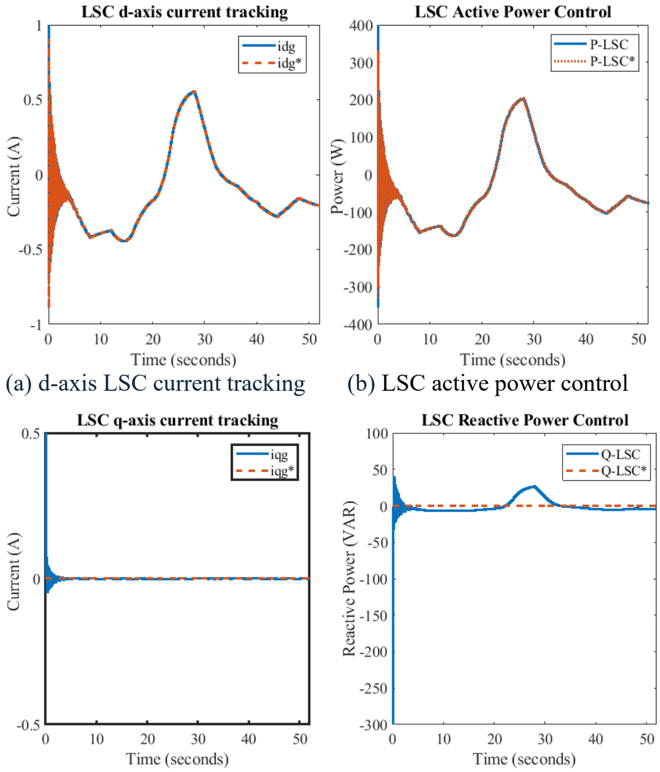

(a) d-axis LSC current tracking (b) LSC active power control
(c) q-axis LSC current tracking (d) LSC reactive power control
Fig. 14. Line side converter active-reactive power control

An accurate regulation of the LSC currents in the dq-axis enables us to have independent control of the active and reactive power flow between the grid and wind turbines.

4. Conclusion

The numerical analysis and the simulation results carried out on a given DFIG agree with each other in many aspects. The PI controllers with anti-wind-up, inner and outer current loops under MPPT algorithms can regulate the system at the set point, and they are able to track dqr for their respective real and reactive power transfer to ensure grid compliance. The machine's active power output is regulated to prevent thermal over-stressing. This limitation becomes particularly important because abnormal grid conditions can lead to an increase in reactive power demand, which in turn places additional stress on the PWM converters. The DC-bus voltage is regulated in a good manner with a small deviation in the attempts of precise control of reactive power, especially at unity power factor. From the results, it can be remarked that a given machine can work optimally under varying wind speeds. The combined results can ensure the compatibility of this small-scale machine to be used in stand-alone/micro-grid/hybrid/grid-connected distributed systems. Confidently, this work can serve as a valuable foundation for further research on wind farms employing DFIGs, particularly in relation to fault scenarios and short-circuit current contribution issues.

Acknowledgement

The authors gratefully acknowledge the Alexander von Humboldt Foundation for providing a scholarship and Technical University of Applied Sciences Würzburg-Schweinfurt (THWS), Center for Electric Power Systems and Renewable Energies in Schweinfurt, Germany, for hosting the first author's research.

References

[1]. Global Wind Energy Council (2025). *Global Wind Report 2025*. Global Wind Energy Council

[2]. Barzigar A, Mujumdar AS, and Hosseinalipour SM, "Review of Seawater Greenhouses: Integrating Sustainable Agriculture into Green Building," Water Conservation Science and Engineering 10(2): 1-31, 2025

[3]. International Energy Agency. (n.d.), *Wind Energy Roadmap: Targets for 2010–2050*. IEA.

[4]. Shah, R., Mithulananthan, N., & Lee, K. Y., ''Grid integration challenges of wind energy: A review.'' IEEE Access (2021), 9, 113–128.

[5]. Sanjari, M. J., & Gooi, H. B., "A review on the integration of wind energy into power systems," Renewable & Sustainable Energy Reviews (2020), 135, 110–119.

[6]. Li, Y., Xu, Z., & Blaabjerg, F., "Advanced control and grid-support functionalities of modern wind power systems: A review," IET Renewable Power Generation (2022), 16(4), 567–582.

[7]. Bin Wu, Mehdi Narimani, "High-Power Converters, and AC Drives," 2nd ed., IEEE Press, New Jersey (2017), USA.

[8]. Milkias Tuka, Mengesha Mamo, "Performance Analysis of Grid Coupled DFIG in a Wind Power System," WSEAS Transactions on Power Systems (2017), Volume 12, 2017.

[9]. Gonzalo Abad, "Power Electronics and Electric Drives for Traction Applications," 1st ed., Mondragon University, Spain (2017), John Wiley & Sons, Ltd.

[10]. G. Abad, J. Lo´pez, M. A. Rodri'guez, L. Marroyo, and G. Iwanski, "Doubly Fed Induction Machine: Modeling and Control for Wind Energy Generation,' 1st ed., IEEE Press and John Wiley & Sons Ltd, USA, New Jersey (2011).

[11]. Lv Y., Zhao X., Mou Z., "Optimization of rotor-side controller parameters in doubly fed induction generators based on an improved NSGA-II." PLoS One 20(6), 2025, https://doi.org/10.1371/journal.pone.0326077

[12]. Yuliang Sun and et al., "Improved robust strategy for unknown disturbances of DC-based DFIG to ensure finite-time stability," Sustainable Energy Technologies and Assessments (2025), 83, DOI: 10.1016/j.seta.2025.104673

[13]. Giri, Jayprakash, Mishra, Neraj Kumar, Patra, Ashish, Shukla, M. K, "Control Strategies of DFIG Technology-based Variable-Speed Wind Turbines-A Review." IOP Conference Series: Earth and Environmental Science (2024), doi:10.1088/1755-1315/1285/1/012007

[14]. Haitham Abu-Rub, Mariusz Malinowski, Kamal Al-Haddad, "Power Electronics for Renewable Energy Systems, Transportation & Industrial Applications," 1st ed., IEEE Press and John Wiley & Sons Ltd, United Kingdom, 2014.

[15]. Hua Huang, Ping JU, Xueping Pan, Yuqing Jin, Xiaoming Yuan, Yuan GAO, "Phase–amplitude model for DFIGs," Journal of Mod. Power Syst. Clean Energy, Springer, 2018.

[16]. Gianto, R., "Constant Power Factor Model of DFIG-Based Wind Turbine for Steady State Load Flow Studies," *Energies (2022)*, https://doi.org/10.3390/en15166077

[17]. Bin Wu; Yongqiang Lang; Navid Zargari; Samir Kouro, "Doubly Fed Induction Generator Based WECS, in Power Conversion and Control of Wind Energy Systems," IEEE (2011), pp.237-274, doi: 10.1002/9781118029008.ch8

[18]. Milkias Berhanu, Roberto Leidhold, "DC Link Voltage and Power Flow Control of a DFIG in Wind Power System," International Journal of Energy (2019), Vol. 13.

[19]. H. Chojaa *et al.*, ''Comparative Study of MPPT Controllers for a Wind Energy Conversion System,'' Lecture Notes on Data Engineering & Communications Technologies (2022), 110, Springer, 300–310, doi:10.1007/978-3-030-94188-8_28

[20]. N. K. Swami Naidu, Member, Bhim Singh, "Experimental implementation of a doubly fed induction generator used for voltage regulation at a remote location," IEEE Transactions on Industry Applications (2016), Vol. 52, 6, pp.5065-5072.

[21]. Medikonda, R. T., & Guo, L., "Performance Evaluation of Artificial Neural Network, Perturb and Observe, and Incremental Conductance MPPT Controllers for Wind Energy Conversion Systems," Electronics (2026), 15(4),853, https://doi.org/10.3390/electronics15040853

[22]. Chen, P.; Han, D.; Li, K.-C., Robust adaptive control of maximum power point tracking for wind power system, IEEE Access (2020), 8, 214538–214550.

[23]. E. Bekiroglu and M. D. Yazar, "MPPT Control of Grid Connected DFIG at Variable Wind Speed," Energies (Basel), vol.15, no. 9, May 2022, doi: 10.3390/en15093146

[24]. Safa Bazrafshan, "A Review of Hybrid Intelligent MPPT Techniques for Grid-Connected Renewable Energy Systems," *TechRxiv (2025),* September 03, 2025, DOI: 10.36227/techrxiv.175691255.53222186/v1

[25]. H. Inapagolla, R. A. and et al., "Metaheuristic Optimization of MPPT Controller for Grid Connected Hybrid Photovoltaic and Wind Distributed Generation System-A Comprehensive Review," *International Conference on Sustainable Communication Networks and Application*, India, 2024, pp. 154-160, doi:10.1109/ICSCNA63714.2024.10863910

[26]. Banerjee, S., & Maity, T., "Exploring Conventional and Recent Algorithms for WECS: A Comprehensive Review of Literature for MPPT," *IETE Technical Review*, 2025, *42*(1), 121–147. https://doi.org/10.1080/02564602.2025.2485899

[27]. Xiangkun Meng, Shiying Ma, Chao Zheng, "Modeling of virtual synchronous controlled-DFIG considering stator voltage control dynamics for transient stability analysis," IJEPES, Vol.156, 2024, doi:10.1016/j.ijepes.2023.109770

Appendix

Table A: Machine Parameters

Machine Type	DFIG, 1kW, 50 Hz, 0.75 cos φ
Rated Voltage	230/400 V
Rated Stator Current	2.0/3.5 A
Rotor/Excitation Voltage	130 V AC/ 24V DC
Rotor rated/Excitation current	4 A, AC /11A, DC
Stator resistance, R_s	1.375 Ω
Rotor resistance	1.45 Ω
Rated torque	5.46 Nm